

# ATP is stored in lamellar bodies to activate vesicular P2X<sub>4</sub> in an autocrine fashion upon exocytosis

Giorgio Fois,<sup>1\*</sup> Veronika Eva Winkelmann,<sup>1\*</sup> Lara Bareis,<sup>1</sup> Laura Staudenmaier,<sup>1</sup> Elena Hecht,<sup>1</sup> Charlotte Ziller,<sup>2</sup> Konstantin Ehinger,<sup>1</sup> Jürgen Schymeinsky,<sup>3</sup> Christine Kranz,<sup>2</sup> and Manfred Frick<sup>1</sup>

<sup>1</sup>Institute of General Physiology and <sup>2</sup>Institute of Analytical and Bioanalytical Chemistry, Ulm University, Ulm, Germany

<sup>3</sup>Immunology and Respiratory Research, Boehringer Ingelheim Pharma GmbH & Co. KG, Biberach an der Riß, Germany

Vesicular P2X<sub>4</sub> receptors are known to facilitate secretion and activation of pulmonary surfactant in the alveoli of the lungs. P2X<sub>4</sub> receptors are expressed in the membrane of lamellar bodies (LBs), large secretory lysosomes that store lung surfactant in alveolar type II epithelial cells, and become inserted into the plasma membrane after exocytosis. Subsequent activation of P2X<sub>4</sub> receptors by adenosine triphosphate (ATP) results in local fusion-activated cation entry (FACE), facilitating fusion pore dilation, surfactant secretion, and surfactant activation. Despite the importance of ATP in the alveoli, and hence lung function, the origin of ATP in the alveoli is still elusive. In this study, we demonstrate that ATP is stored within LBs themselves at a concentration of ~1.9 mM. ATP is loaded into LBs by the vesicular nucleotide transporter but does not activate P2X<sub>4</sub> receptors because of the low intraluminal pH (5.5). However, the rise in intravesicular pH after opening of the exocytic fusion pore results in immediate activation of vesicular P2X<sub>4</sub> by vesicular ATP. Our data suggest a new model in which agonist (ATP) and receptor (P2X<sub>4</sub>) are located in the same intracellular compartment (LB), protected from premature degradation (ATP) and activation (P2X<sub>4</sub>), and ideally placed to ensure coordinated and timely receptor activation as soon as fusion occurs to facilitate surfactant secretion.

## INTRODUCTION

Extracellular nucleotides are widely recognized to stimulate cellular secretion via activation of either ionotropic P2X or G protein-coupled P2Y receptors (Novak, 2011; Burnstock et al., 2014). In many cells activation of these receptors leads to an increase in the intracellular Ca<sup>2+</sup> concentration ([Ca<sup>2+</sup>]<sub>i</sub>), triggering exocytic fusion of secretory vesicles with the plasma membrane (PM; Erb et al., 2006; Surprenant and North, 2009). In the classical model, this Ca<sup>2+</sup> signal determines the number of vesicles fusing with the PM and releasing their content, thereby regulating the amount of cellular secretion. However, secretion can also be regulated during the so-called exocytic postfusion phase, after vesicle-PM fusion. It has been demonstrated that regulation of fusion pore expansion and/or contractile forces acting on the fused vesicles determine the composition and quantity of cellular secretion in cells containing large secretory granules and the secreting of bulky vesicle contents (Breckenridge and Almers, 1987; Obermüller et al., 2005; Vardjan et al., 2009; Porat-Shliom et al., 2013). Recent evidence suggests that P2X receptors also play a role in secretion during this postfusion phase. We have demonstrated that vesicular P2X<sub>4</sub> receptors facilitate the secretion and activation of pulmonary surfactant in the alveoli of the lung after vesicle-PM fusion (Miklavc et al., 2011; Dietl et al., 2012; Thompson et al., 2013).

Pulmonary surfactant is a poorly soluble, lipoprotein-like substance that is stored as densely packed membranous structures in large secretory lysosomes termed lamellar bodies (LBs). Upon stimulation, surfactant is secreted into the alveolar lumen via exocytosis of LBs. However, because of its bulky nature, surfactant remains entrapped within fused vesicles for minutes after fusion. Secretion is restricted by the slowly expanding fusion pore that acts as a mechanical barrier for the release (Singer et al., 2003; Dietl and Haller, 2005; Miklavc et al., 2012). This fusion pore expansion is regulated by Ca<sup>2+</sup> (Haller et al., 2001; Neuland et al., 2014).

We have recently described that extracellular ATP triggers fusion-activated Ca<sup>2+</sup> entry (FACE) via P2X<sub>4</sub> receptors after the fusion of LBs with the PM (Miklavc et al., 2011). P2X<sub>4</sub> receptors are expressed on the limiting membranes of LBs and therefore protected from premature activation (Xu et al., 2014). The vesicular P2X<sub>4</sub> receptors are exposed to the extracellular space after LB exocytosis. Subsequent receptor activation by extracellular ATP results in a transient, local Ca<sup>2+</sup> influx at the site of LB fusion, provides the Ca<sup>2+</sup> necessary for fusion pore expansion, and facilitates surfactant release. (Miklavc et al., 2011; Neuland et al., 2014). Moreover, *in vivo*, FACE is restricted to the apical side of AII cells (alveolar lumen). As a consequence, FACE triggers vec-

\*G. Fois and V.E. Winkelmann contributed equally to this paper. Correspondence to Manfred Frick: manfred.frick@uni-ulm.de

© 2018 Fois et al. This article is distributed under the terms of an Attribution-Noncommercial-Share Alike-No Mirror Sites license for the first six months after the publication date (see <http://www.rupress.org/terms/>). After six months it is available under a Creative Commons License (Attribution-Noncommercial-Share Alike 4.0 International license, as described at <https://creativecommons.org/licenses/by-nc-sa/4.0/>).



torial, apical-to-basolateral ion transport across ATII cells and thereby drives apical (luminal) fluid resorption in the alveolus. This results in temporary thinning of the alveolar lining fluid layer (“hypophase”) and facilitates adsorption of newly released surfactant into the air–liquid interface (Thompson et al., 2013).

Despite the importance of ATP for alveolar physiology, the origins of ATP in the alveoli are still elusive. It has been reported that ATP is present in the pulmonary hypophase (Patel et al., 2005); however, the estimated concentration under resting conditions is in the low nanomolar range (Bove et al., 2010), well below the concentration at half-maximal response ( $EC_{50}$ ) values for  $P2X_4$  or  $P2Y_2$  activation (Lazarowski et al., 1995; North, 2002; Brunschweiler and Müller, 2006). A possible reason for this low concentration is rapid hydrolysis of extracellular ATP in the hypophase (Lazarowski et al., 2011; Lazarowski, 2012). Hence, a tight temporal and spatial coordination between ATP release and ATP demand (i.e.,  $P2$  receptor activation) could be essential for providing appropriate concentrations of ATP. Although several mechanisms for ATP release have been identified in airway epithelia (Ransford et al., 2009; Kreda et al., 2010; Mishra et al., 2011; Okada et al., 2011; Seminario-Vidal et al., 2011), little is known about mechanisms and/or regulation of ATP release in the alveoli. In particular, local ATP release within individual alveoli may provide an ideal mechanism to gradually adapt local surfactant secretion and fluid transport to local demands.

In this study, we therefore wanted to address the question whether ATII cells release ATP. Specifically, we investigated whether ATP release is spatially and temporarily coupled to LB exocytosis and whether it provides the necessary ATP concentrations for activation of FACE. Our results clearly demonstrate that (a) ATP is stored in LBs; (b) ATP accumulation in LBs depends on transport via vesicular nucleotide transporter (VNUT); and (c) the rise in pH upon exocytic opening of the fusion pore results in  $P2X_4$  activation by vesicular ATP.

In summary, our data demonstrate that agonist (ATP) and receptor ( $P2X_4$ ) are located in the same intracellular compartment (LB), protected from premature degradation (ATP) and activation ( $P2X_4$ ), but ideally suited to result in the most efficient receptor activation to induce FACE and facilitate fusion pore dilation, surfactant secretion, and fluid resorption from alveoli upon LB exocytosis.

## MATERIALS AND METHODS

### Materials

Anti-VNUT pAB (serum) was a gift from Y. Moriyama (Okayama University, Okayama City, Japan); anti-P180 lamellar body protein (ABCa3) mAB was purchased from Abcam. Fluorescence-labeled secondary antibodies

and fluorescent dyes were obtained from Molecular Probes (Thermo Fisher Scientific). All chemicals were purchased from Sigma-Aldrich unless stated otherwise.

### Cell isolation and primary ATII cell culture

ATII cells were isolated from Sprague-Dawley rats according to the procedure of Dobbs et al. (1986) with minor modifications as recently described (Miklavc et al., 2010). After isolation, cells were seeded on glass coverslips or 8-well chambers (Ibidi), cultured in MucilAir (Epithelix), and used for experiments for up to 72 h after isolation.

### Experimental conditions

For all experiments, cells were kept in bath solution (mM: 140 NaCl, 5 KCl, 1  $MgCl_2$ , 2  $CaCl_2$ , 5 glucose, and 10 HEPES, pH 7.4) unless stated otherwise. To efficiently induce LB fusions, ATII cells were treated with UTP (100  $\mu$ M), PMA (300 nM), or both, all known and potent agonists for LB fusion and surfactant secretion (Frick et al., 2001; Miklavc et al., 2011). Concentrations were chosen to induce maximum fusion response.

### Plasmids and adenoviruses

Adenoviruses encoding  $P2X_4$ -EGFP (WT) were recently described (Miklavc et al., 2011); original constructs were a gift from R.D. Murrell-Lagnado (University of Cambridge, Cambridge, England, UK). Plasmid expressing VNUT-GFP (Oya et al., 2013) was a gift from T. Tsuboi (University of Tokyo, Tokyo, Japan).

Original constructs expressing the ATeam ATP sensors (Imamura et al., 2009) were a gift from H. Imamura (Kyoto University, Japan). ATeam3.10-GL-GPI was generated according to Keller et al. (2001) and resulted in a GPI-anchored version of ATeam3.10. In brief, the signal sequence of lactase-phlorizin hydrolase was inserted 5' of ATeam3.10 sequence, and the GPI-attachment signal of lymphocyte function-associated antigen 3 was attached to the 3' end of ATeam3.10 via a 12x glycine linker, resulting in LPH-ATeam3.10-12xGly-GPI. Cloning was performed using In-Fusion HD Cloning kit (Clontech). The Nucleofector 4D system (Lonza) was used for plasmid transfection of primary ATII cells.

VNUT (SLC17A9) shRNA adenovirus was constructed based on the shRNA cassette design described by Gou et al. (2008). In brief, four shRNA sequences targeting rat VNUT CDs and 3' UTR (accession no. NM\_001108613.1) were chosen with BLOCK-iT RNAi Designer (Thermo Fisher Scientific). Sequences were BLASTed against rat genome to check for off-target binding. To monitor transduction efficiency, a triple SV40 nuclear localization sequence was added to the 3' end of BFP, and the construct was cloned into the cytomegalovirus (CMV)-controlled site of pO6A5-CMV (Sirion Biotechnologies). 7SK and mU6 RNA polymerase promoters were then introduced 5' of the

CMV promoter sequence, directed toward each other. The shRNA cassette containing the four shRNAs plus hU6 and H1 promoters was synthesized (GeneArt/Thermo Fisher Scientific) and introduced between the mU6 and 7SK promoters, leading to the final construct (5' to 3'; s, sense; as, antisense) mU6 (s), shRNA1 (s), linker, shRNA2 (as), hU6 promoter (as), H1 promoter (s), shRNA3 (s), linker, shRNA4 (as), 7SK (as), CMV (s), BFP (s), and 3xNLS (s). All cloning steps were controlled by sequencing. Adenovirus was then produced according to the manufacturer's protocol and purified using ViraBind Adenovirus Purification kit (Cell Biolabs). Viral transduction efficiency was determined by the expression of nuclear BFP and averaged  $72 \pm 4.1\%$  transduced cells after 24 h. Knockdown efficiency was determined by quantitative RT-PCR.

#### Semiquantitative RT-PCR

Total RNA was isolated from  $10^6$  ATII cells 24 h after isolation using RNeasy MiniKit (Qiagen). Reverse transcription was performed on 0.8–1.3  $\mu\text{g}$  total RNA using SuperScript VILO cDNA synthesis kit according to manufacturer's protocol. The following validated QuantiTect primer assay (Qiagen) was used to determine VNUT (SLC17A9) expression: Rn\_Slc17a9\_1\_SG. Amplification was performed on a Realplex2 Mastercycler (Eppendorf) using the Express SYBR GreenER PCR Supermix. Each reaction was performed on cDNA from  $\geq 3$  independent isolations (cDNAs were used at 1-, 10-, and 100-fold dilutions). Specificity of PCR reactions was confirmed by melting point analysis of PCR products. Realplex software (Eppendorf) was used for data acquisition and analysis. Correction for PCR performance as well as quantification relative to housekeeping gene HMBS (Rn\_HMBS\_1\_SG) was performed as described (Pfaffl, 2001).

#### Western blotting

$10^6$  ATII cells were washed twice in PBS, solubilized in lysis buffer, separated on SDS-PAGE, and transferred to nitrocellulose. Immunodetection of VNUT was performed using  $\alpha$ -VNUT pAB serum (1:200) and chromogenic detection of alkaline phosphatase-labeled secondary antibody (WesternBreeze anti-rabbit; Invitrogen).

#### Immunofluorescence

For immunofluorescence staining, cells were washed twice in Dulbecco's PBS (DPBS; pH 7.4; Biochrom), fixed for 20 min in 4% PFA in DPBS, washed twice in DPBS, fixed for 10 min in ice-cold DPBS:MeOH (1:1), washed trice in DPBS, and permeabilized for 10 min with 0.2% saponin and 10% FBS (Thermo Fisher Scientific) in DPBS. Cells were stained with primary (1:100) and secondary (1:400) antibodies in PBS, 0.2% saponin, and 10% FBS. Images were taken on an inverted confocal

microscope (Leica TCS SP5) using a 63 $\times$  lens (Leica HCX PL APO lambda blue 63.0  $\times$  1.40 oil UV). Images for the green (Alexa Fluor 488) and red (Alexa Fluor 568) channels were taken in sequential mode using appropriate excitation and emission settings.

#### Fluorescent ATP uptake

Primary ATII cells were incubated with either 10  $\mu\text{M}$  BODIPY FL ATP or 10  $\mu\text{M}$  mant-ATP (Thermo Fisher Scientific) for 3 h in MucilAir medium, after 2.5 h LTR (100 nM) was added to the medium. Cells were then washed three times with bath solution (and maintained in bath solution) and immediately mounted on a Cell Observer inverse microscope (Zeiss) for analysis of fluorescence. All images were acquired at identical settings (e.g., magnification, gain, excitation). Mean fluorescence of individual LBs was analyzed within regions encircling individual LBs (see Fig. 4 A and Fig. S5).

#### Luciferase assay to quantify ATP release

Primary  $10^6$  ATII cells were seeded into wells of a 96-well plate (Sarstedt) and maintained in MucilAir medium. 48 h after seeding, the medium was exchanged with fresh medium containing 100  $\mu\text{M}$  ARL 67156 (Tocris). The cells were then incubated with 10  $\mu\text{M}$  Evans Blue or 100 nM bafilomycin A1 for 170 min. Cells were stimulated with 300 nM PMA or 100  $\mu\text{M}$  UTP for 10 min, and supernatants were collected for ATP quantification. ATP release was quantified using ATP Determination kit (Thermo Fisher Scientific) according to the manufacturer's protocol. Luminescence was recorded in an Infinite M200 plate reader (Tecan).

#### ATP biosensors and quantification of ATP release from single LBs

ATP microbiosensors were prepared by immobilizing glucose oxidase (from *Aspergillus niger*; 1,500,000 U/g; Sigma-Aldrich Chemie) and hexokinase (from yeast; 2,500 IU solid; Calbiochem, Merck) in a poly(benzoxazine) layer (Ziller et al., 2017) Pt microelectrodes with a radius of 25  $\mu\text{m}$  were modified by electrodeposition using mixtures of BA-TEPA and GOD/HEX in a ratio of 1:2.5 wt/wt; the activity ratio for the two enzymes was 1:1. The synthesis of the precursor was prepared as previously described (Andronescu et al., 2014). Depositions were performed with a potential pulse sequence of 1.7 V/0.05 s, 0.0 V/0.5 s, and 14 repetitions of the pulse cycle. Calibrations were performed in Tris buffer at a potential of 0.7 V versus Ag/AgCl (3 M KCl) with addition of glucose and ATP aliquots, respectively. All electrochemical experiments were performed with a three-electrode configuration with the microelectrode, microelectrode assembly, or microbiosensor as working electrode, Pt as counterelectrode (CE), and Ag/AgCl (3 M KCl) reference electrode unless otherwise stated. Tris-buffer bath solution (TBS: same composition as nor-

mal bath solution) was used instead of HEPES for all electrochemical experiments. Tris is used to avoid hydrogen peroxide formation caused by photooxidation (Masson et al., 2008). Glucose oxidase catalyzes the oxidation of glucose that is present in the medium. This leads to the formation of hydrogen peroxide as a byproduct when oxygen is the electron acceptor. Hydrogen peroxide is then oxidized at the sensor surface, leading to an increase in current, which represents the baseline signal. If ATP is present in solution (e.g., is released by the cells), hexokinase catalyzes the phosphorylation of glucose, resulting in ADP and glucose-6-phosphate, therefore reducing the glucose concentration available for the glucose oxidase-catalyzed process. Thus, the decrease in hydrogen peroxide reflected by a decrease in faradaic current is proportional to the concentration of ATP (Fig. S4).

To quantify ATP release from single LBs upon exocytosis, primary ATII cells were incubated with 0.25  $\mu$ M LysoTracker Green (LTG) for 15 min in MucilAir medium, washed twice, and maintained in Tris buffer. Cells were then mounted on a customized stage of an inverted fluorescence microscope (IX81; Olympus America) combined with the scanning electrochemical microscope. To position the ATP microbiosensor at a fixed, defined distance from the cell surface, a dual-electrode assembly is used, with one electrode modified with the enzyme-containing layer (WE1) and a bare second microelectrode (WE2) for recording current–distance curves. Positioning was achieved via recording current–distance curve with WE2 biased at  $-0.7$  V versus Ag/AgCl quasireference electrode (AgQRE) for recording the oxygen reduction current. The approach was stopped at a normalized current value of 0.8, corresponding to tip–sample distances of 30  $\mu$ m. After positioning, the working electrode (W2) was disconnected, and WE1 was biased at 0.7 V versus AgQRE. After a stable baseline was obtained, cells were stimulated with PMA (300 nM) and ionomycin (1  $\mu$ M). Images were taken at a rate of 0.25 Hz using a Snap Camera EZ CCD (Photometrics) every 4 s to detect individual LB fusions using ImageJ software (v.2.0.0; National Institutes of Health). Fusion events were then correlated to changes in the faradaic current. To ensure that the ATP microbiosensors were functional throughout the experiment, aliquots of ATP and glucose were added after each experiment.

#### Live-cell fluorescence imaging of FACE

FM1-43 experiments were performed on an iMic digital microscope (Till Photonics) or a Cell Observer inverse microscope (Zeiss). For combined fura-2 and FM1-43 experiments, cells were seeded on 13-mm coverslips, loaded for 20 min with fura-2 AM (3  $\mu$ M) before the start of the experiment, washed three times in DPBS, and mounted in a inverse manner on a drop of bath solution containing 300 nM PMA and 1  $\mu$ M FM1-43 within

a glass coverslip (Ibidi). This upside-down mounting resulted in a minimum liquid layer on the apical side of the cell layer. Imaging was started immediately after mounting of cells. Cells were illuminated for 50 ms at a rate of 0.3–0.5 Hz at each excitation wavelength (340 and 380 nm for Fura-2; 480 nm for FM1-43). 495-nm (Observer) and 520-nm (iMic) dichroic mirrors were used to deflect excitation light. Images were acquired using MetaFluor (Molecular Devices) or iMic Online Analysis (Till Photonics).

#### Image analysis and data presentation

Images were analyzed using MetaFluor Analyst (Molecular Devices), iMic Offline analysis software (Till Photonics), and ImageJ, as recently described (Miklavc et al., 2011). To eliminate potential interference with Fura-2 ratio calculations in combined fura-2 and FM1-43 experiments, fura-2 fluorescence was determined in ring-like (perivesicular) regions of interest (800 to 1000 nm wide) surrounding the fused, FM1-43-stained LB. Onset of the calcium rise was specified as the time point when the increase in the fura-2 ratio exceeded two times its SD. The peak amplitude for fura-2 signals was specified as the difference between fura-2 ratio values of the last time point before onset of FACE and the maximum value within 10 s thereof (Miklavc et al., 2011). Diffusion of FM1-43 into newly fused LBs was analyzed as a direct means to compare fusion pore opening after LB fusion under various conditions. Because of the slow kinetics of FM1-43 labeling of fused vesicles, we analyzed the initial slope (10 s after fusion) of the increase of FM1-43 fluorescence (Miklavc et al., 2011).

#### Statistics

MS Excel (Microsoft) and Prism 6 (GraphPad) were used for statistics, curve fitting, and graph design. Unless otherwise stated, all data are presented as mean  $\pm$  SEM. Statistical significance was determined using ANOVA (with Bonferroni's correction) for multiple comparisons and an unpaired, two-tailed Student's *t* test for comparison of two independent samples. Data were considered significant if the *p*-value was  $<0.05$ .

#### Online supplemental material

Fig. S1 shows expression and knockdown of in primary ATII cells. Fig. S2 shows treatment with Evans Blue, VNUTshRNA, bafilomycin A, or NH<sub>4</sub>Cl does not affect LB fusion activity. Fig. S3 shows calibration of genetically encoded ATP sensors expressed in the outer leaflet of PM. Fig. S4 shows dual-electrode ATP sensors to quantitatively analyze ATP release from individual LBs. Fig. S5 shows inhibition of VNUT and dissipation of  $\Delta\psi$  but not dissipation of the vesicular proton gradient ( $\Delta$ pH) impair BODIPY FL ATP uptake into LBs.

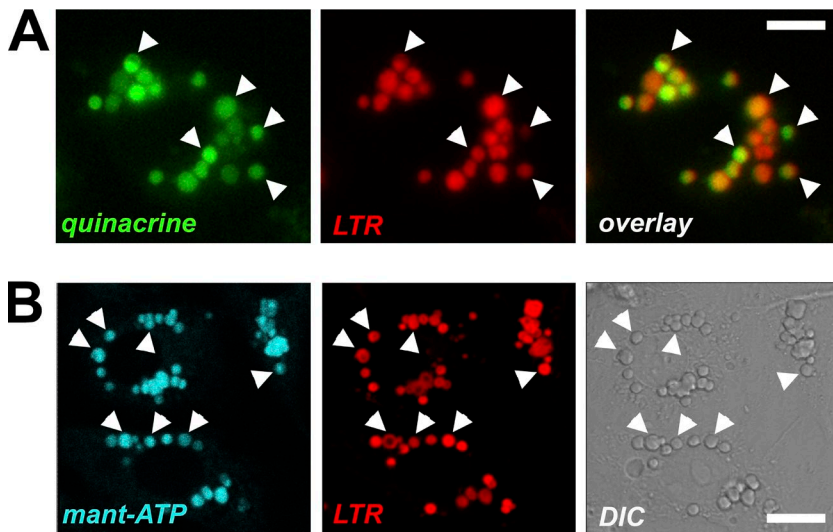


**Figure 1. ATP is stored in LBs. (A)** Staining of primary ATII cells with quinacrine and LTR (a marker for LBs), indicating the presence of intravesicular ATP in LBs (arrowheads). Bar, 10 μm. **(B)** ATII cells were incubated with mant-ATP for 1 h and labeled with LTR. Mant-ATP is enriched in LBs (arrowheads). Bar, 10 μm.

## RESULTS

### ATP is stored in LBs

Significant amounts of ATP have been found in a variety of secretory vesicles, including lysosome-related organelles (Bodin and Burnstock, 2001; Praetorius and Leipziger, 2009; Haanes and Novak, 2010; Lazarowski et al., 2011). Moreover, ATII-like A549 cells release ATP upon stimulation, likely via exocytosis (Tatur et al., 2008; Ramsingh et al., 2011). We therefore initially investigated whether LBs in primary ATII cells also contain ATP. Quinacrine, a dye known to be associated with ATP stores (Sorensen and Novak, 2001), selectively and strongly labels LBs (identified by the strong Lysotracker Red [LTR] staining), indicating the presence of intravesicular ATP (Fig. 1 A). In a second set of experiments, we used fluorescently labeled ATP to further validate and monitor uptake of ATP into LBs. Mant-ATP (Fig. 1 B), as well as BODIPY FL ATP (Fig. 4 A), accumulated in LBs, and within 3 h of incubation, a strong signal—by far exceeding cytoplasmic staining—could be observed in LBs.

Additional evidence for endogenous ATP in LBs comes from experiments in which neutralization of intravesicular pH results in a selective  $\text{Ca}^{2+}$  efflux from LBs. It has been recently demonstrated that endolysosomal  $\text{P2X}_4$  forms channels activated by luminal ATP in a pH-dependent manner (Huang et al., 2014) and that endolysosomal  $\text{P2X}_4$  activation by alkalinization of endolysosome lumen resulted in  $\text{Ca}^{2+}$  release from endolysosomes (Cao et al., 2015). Neutralization of the intra-LB pH with 10 mM  $\text{NH}_4$  (Fois et al., 2015) resulted in a transient rise of the cytoplasmic  $\text{Ca}^{2+}$  concentration around LBs (Fig. 2). This is likely caused by activation of  $\text{P2X}_4$  receptors by intravesicular ATP, as overexpression of the WT  $\text{P2X}_4$  ( $\text{P2X}_4\text{-mCherry}$ ; Fig. 2 A) significantly increased the amplitude of the  $\text{Ca}^{2+}$  signal within a 1-μm perivesicular region around

fusion LBs compared with nontransduced cells ( $P = 0.0003$ ; Fig. 2 B).

### ATP uptake into LBs depends on VNUT

Next, we aimed at identifying the underlying mechanisms for loading of ATP into LBs. Increasing evidence suggests that accumulation of ATP in lysosomes and secretory vesicles depends on a VNUT (aka SLC17A9; Sawada et al., 2008; Oya et al., 2013; Sesma et al., 2013; Cao et al., 2014); however, some studies also propose alternative mechanisms, including  $\text{H}^+$ -ATPase-dependent uptake of ATP into secretory vesicles (Imura et al., 2013). Therefore, we investigated whether accumulation of ATP within LBs was also VNUT dependent. First, we ascertained the expression of VNUT in ATII cells. RT-PCR data (Fig. S1 A), as well as expression analysis by Western blot (Fig. 3 A), revealed that VNUT is expressed in ATII cells. Importantly, expression is not a result of dedifferentiation of ATII cells in culture. There is no difference in transcript and protein levels between freshly isolated cells (30 min after isolation) and cells in culture for up to 48 h. Immunofluorescent staining of ATII cells for VNUT further confirmed that it is primarily localized on LBs and colocalizes with P180 LB protein (ABCA3; Fig. 3 B). VNUT-GFP, expressed in primary ATII cells, was also almost exclusively localized on LBs (Fig. 3 C).

We next performed functional assays to test VNUT-dependent loading of ATP into LB. To this end, we incubated primary ATII cells with fluorescent ATP (BODIPY FL ATP) for 3 h and analyzed accumulation of BODIPY FL ATP in LBs under unperturbed control conditions, in the presence of VNUT inhibitor Evans Blue (100 μM), or after knockdown of VNUT expression by VNUT shRNA treatment for 72 h (Fig. 4, A and B; and Fig. S5). Treatment of primary ATII cells with VNUT shRNA resulted in a  $69.4 \pm 7.1\%$  reduction of VNUT transcript levels (Fig. S1 B) and almost complete de-

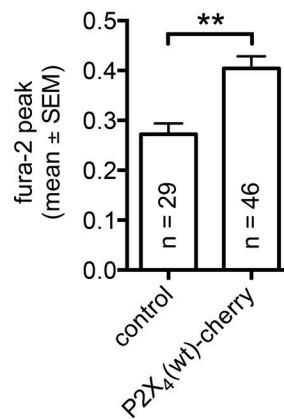
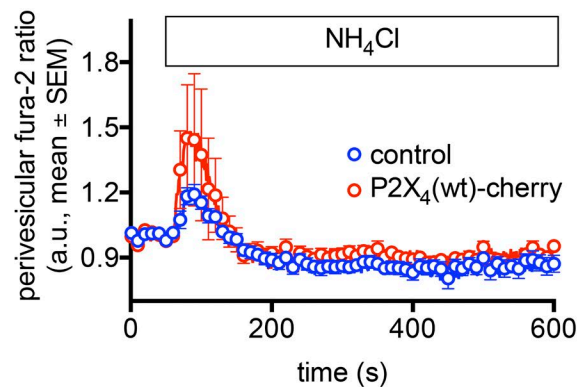
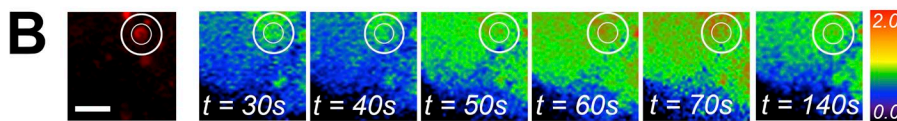
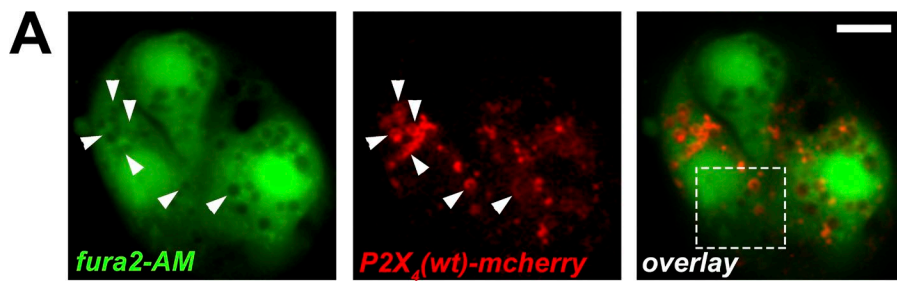


**Figure 2. Alkalinization-induced  $\text{Ca}^{2+}$ -release from LBs is P2X4 dependent.** (A) ATII cells labeled with fura 2-AM and expressing WT P2X4 tagged with mCherry (P2X<sub>4</sub>(WT)-mCherry). P2X<sub>4</sub> is predominantly localized on LBs (arrowheads). Bar, 10  $\mu\text{m}$ . (B) Top left: Image depicts the boxed area in A and highlights the perivesicular region (area between circles) around a P2X<sub>4</sub>(WT)-mCherry-positive LB where changes in the fura-2 ratio were recorded. Image series illustrates changes in fura-2 ratio after addition of 10 mM NH<sub>4</sub>Cl (at  $t = 40$  s) in the same area as the image on the left. Bar, 5  $\mu\text{m}$ . Bottom left: Normalized fura-2 ratios measured within a 1- $\mu\text{m}$  perivesicular region around individual LBs (as illustrated in A, top) in control cells (blue) and cells (over)expressing P2X<sub>4</sub>(WT)-mCherry (red) treated with 10 mM NH<sub>4</sub>. Data represent means from 14 and 11 cells, respectively. Right: Quantification of the NH<sub>4</sub>-induced fura-2 peak amplitude. Overexpression of P2X<sub>4</sub>(WT)-mCherry, significantly increased amplitude (\*\*,  $P = 0.0003$ ).

pletion of VNUT from LB membranes in transduced cells (as identified by nuclear blue fluorescent protein

[BFP] staining; Fig. S1 C) after 72 h. Analysis of the mean BODIPY FL ATP fluorescence in individual LBs

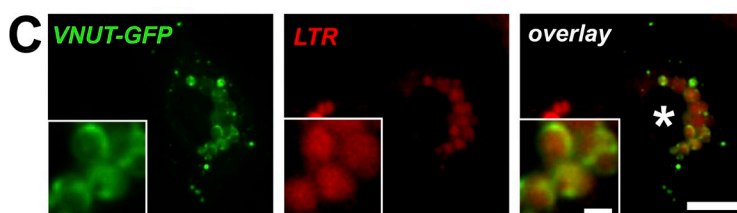
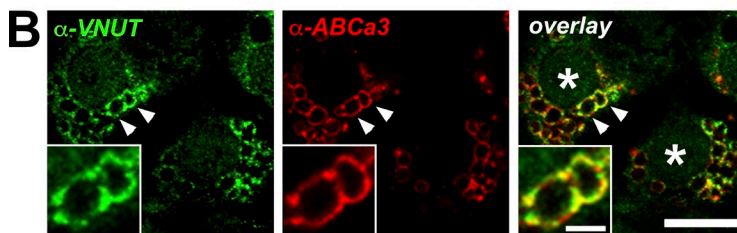
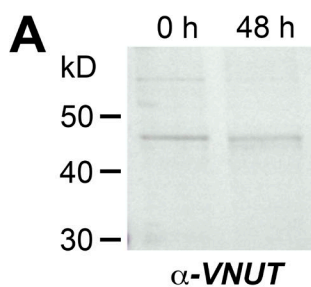


**Figure 3. VNUT is expressed in isolated ATII cells and localized on the LB membrane.** (A) Western blot of VNUT from ATII cells freshly isolated and 48 h after isolation confirms that expression of VNUT is not altered in cultured cells. (B) VNUT (green) is primarily localized on LB membranes (arrowheads) as detected by indirect immunofluorescence and confirmed by colocalization with P180 lamellar body protein (red,  $\alpha$ -ABCa3). Asterisks denote nuclei of individual primary ATII cells. Bar: 10  $\mu\text{m}$ ; (inset) 2  $\mu\text{m}$ . (C) VNUT-GFP (green) localizes to the membrane of LBs (LTR, red) in primary ATII cells. Asterisk denotes nuclei of primary ATII cell. Bar: 10  $\mu\text{m}$ ; (inset) 2  $\mu\text{m}$ .

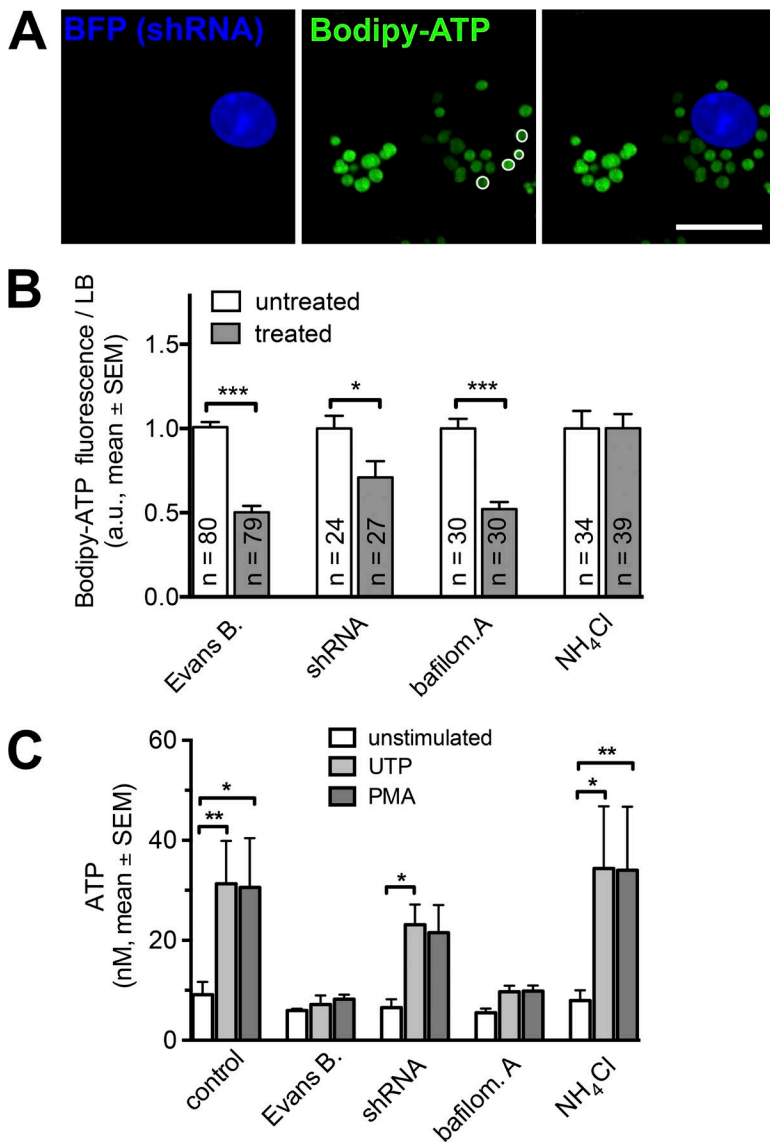


**Figure 4. ATP uptake into LBs depends on VNUT.** (A) Images illustrating loading of BODIPY FL ATP (green) into individual LBs (encircled). BODIPY FL ATP uptake was reduced in cells expressing VNUT-shRNA. Cells expressing VNUT-shRNA are identified by coexpression of nuclear BFP (blue). Bar, 10  $\mu$ m. (B) Normalized BODIPY FL ATP fluorescence in individual LBs after a 3-h incubation period in the absence (untreated) or presence (treated) of VNUT inhibitor Evans Blue (100  $\mu$ M), knockdown of VNUT expression by VNUT shRNA treatment for 72 h, inhibitor of H<sup>+</sup>-ATPase (100 nM bafilomycin A, 4 h), or treatment with NH<sub>4</sub>Cl (10 mM). BODIPY FL ATP fluorescence was analyzed within regions encircling individual LBs (as illustrated by circles in A). *n*, number of cells analyzed. \*, *P* < 0.05; \*\*\*, *P* < 0.001. (C) Quantification of ATP release from ATII cells after stimulation of LB exocytosis with either 100  $\mu$ M UTP or 300 nM PMA for 10 min in control cells or cells treated with VNUT inhibitor Evans Blue (100  $\mu$ M, 3 h), VNUT-shRNA (72 h), bafilomycin A (100 nM, 4 h), or NH<sub>4</sub>Cl (10 mM, 3 h). Data represent means  $\pm$  SEM from  $\geq$  4 individual cell isolations. \*, *P* < 0.05; \*\*, *P* < 0.01.

revealed that inhibition ( $49.8 \pm 3.9\%$ , *P* = 0.0001) and knockdown of VNUT expression ( $29.0 \pm 9.6\%$ , *P* = 0.02) resulted in a significant reduction of BODIPY FL ATP uptake into LBs. It has also been suggested that ATP transport by VNUT depends on vesicular membrane potential ( $\Delta\psi$ ), but not on vesicular proton gradient ( $\Delta$ pH; Sawada et al., 2008; Moriyama et al., 2017). We therefore also performed experiments in the presence of either 100 nM bafilomycin A (added 4 h before addition of BODIPY FL ATP) to selectively dissipate  $\Delta\psi$  or 10 mM NH<sub>4</sub>Cl to selectively dissipate  $\Delta$ pH. Dissipating  $\Delta\psi$  resulted in a reduction of BODIPY FL ATP uptake into LBs ( $47.9 \pm 4.3\%$ , *P* = 0.0001), similar to inhibition of VNUT, whereas breakdown of  $\Delta$ pH had no effect on BODIPY FL ATP uptake (*P* = 0.99; Fig. 4 B).

#### ATP is released from individual LBs upon exocytosis

To test whether ATP is released from LBs upon exocytosis, we quantitatively analyzed ATP release from

ATII cells after stimulation of LB exocytosis with either 100  $\mu$ M UTP or 300 nM PMA for 10 min (Frick et al., 2001; Miklavc et al., 2011). Stimulation of primary ATII cells with either UTP or PMA significantly increased the concentration of ATP in the supernatant from  $9.1 \pm 2.6$  to  $31.3 \pm 8.6$  nM (*P* = 0.007) and  $30.6 \pm 9.8$  nM (*P* = 0.01), respectively (*n* = 7 individual cell isolations). In line with the BODIPY FL ATP uptake assays, inhibition of VNUT (100  $\mu$ M Evans Blue for 3 h) abolished significant releases of ATP after stimulation with UTP (*P* = 0.95, *n* = 4) or PMA (*P* = 0.20, *n* = 4). The amount of ATP released after knockdown of VNUT (shRNA) was also less than under control conditions,  $23.1 \pm 4.0$  nM (*n* = 5) after UTP stimulation and  $21.5 \pm 5.5$  nM (*n* = 5) after PMA stimulation, respectively. However, this effect was much less pronounced than after VNUT inhibition. This is probably caused by the inefficient transduction efficiency (mean of  $72 \pm 4.1\%$  of cells) in primary ATII cells or breakdown of  $\Delta\psi$  (bafilomycin A). Dissipation

of  $\Delta\psi$  abolished ATP release almost completely after stimulation with either UTP or PMA. Dissipation of  $\Delta\text{pH}$  with  $\text{NH}_4\text{Cl}$  did not affect ATP. ATP concentrations in the supernatant reached similar levels to control conditions after stimulation with UTP ( $34.0 \pm 12.6$  nM,  $n = 5$ ) or PMA ( $34.4 \pm 12.5$  nM,  $n = 6$ ; Fig. 4 C).

None of the inhibitor treatments affected the rate of LB exocytosis after stimulation. Neither the fraction of cells responding with at least one LB fusion within 10 min of stimulation (% responders, Fig. S2 A) nor the mean number of fusions within these responsive cells (Fig. S2 B) was significantly altered.

To further substantiate that ATP is indeed released from individual LBs and exclude the possibility that the observed ATP release is caused by other molecular mechanisms (Lazarowski et al., 2011), we established assays to directly correlate LB exocytosis and ATP release. In a first set of experiments, we used a genetically encoded ATP sensor (Imamura et al., 2009) that is attached to a glycosyl phosphatidyl inositol (GPI) anchor to selectively localize it in the outer leaflet of the PM (ATeam3.10-GL-GPI; Fig. 5 A). Expression of ATeam3.10-GL-GPI in ATII enabled detection of changes in the extracellular ATP concentration (Fig. 5 B and Fig. S3) with high temporal and spatial resolution. We performed experiments in which we simultaneously recorded LB fusion events (FM1-43) and changes in the extracellular ATP concentration (YFP/CFP ratio). These experiments revealed that LB fusions in close proximity to the ATP sensors resulted in an increase of the YFP/CFP ratio (Fig. 5 C), suggesting local ATP release from the LB upon fusion and fusion pore opening ( $n = 4$  fusions). No change in the YFP/CFP ratio was observed in the absence of LB fusions within  $20 \mu\text{m}$  of the ATP sensors.

In a second set of experiments, we used microelectrochemical ATP sensors (Fig. S4) in combination with live imaging experiments to simultaneously monitor individual LB fusion events and changes in the ATP concentration (Fig. 5 B). These experiments allowed direct correlation between fusion events and changes in ATP concentration in close proximity to the cells (Fig. 5 C). After stimulation of LB fusion with 300 nM PMA, we observed a mean of  $7.39 \pm 2.13$  fusions under the electrode area ( $r = 25 \mu\text{m}$ ), which resulted in a mean increase in the ATP concentration in the small volume under the ATP-sensing electrode assembly of  $0.42 \pm 0.10 \mu\text{M}$  ( $n = 7$  experiments). Based on the calculation of the volume ( $58,904.8 \mu\text{m}^3 = 58.90 \text{ pl}$ ) defined by the area of the electrode assembly and the distance between the cells and the enzyme-containing polymer layer ( $30 \mu\text{m}$ ), this equals an ATP release of  $0.025 \pm 0.006 \text{ fmol}$ , equaling a release of  $3.40 \pm 0.81 \text{ amol ATP per LB fusion}$ . Assuming a mean LB diameter of  $1.5 \mu\text{m}$ , this would correlate to a mean concentration of  $1.92 \pm 0.45 \text{ mM ATP}$  inside a single LB.

### Vesicular ATP stimulates FACE upon LB exocytosis

In a final experiment, we investigated whether vesicular ATP can activate  $\text{P2X}_4$  receptors and stimulate FACE in an “autocrine” fashion upon LB exocytosis. If sufficient ATP is present in individual LBs, the rise in intravesicular pH after opening of the exocytic fusion pore results in immediate activation of vesicular  $\text{P2X}_4$  by vesicular ATP. Therefore, we performed experiments monitoring individual LB fusion events and rises in intracellular  $\text{Ca}^{2+}$  in primary ATII cells stimulated with 300 nM PMA (Fig. 6 A; Frick et al., 2001; Miklavc et al., 2011). To restrict rapid dilution of LB ATP in the extracellular solution and mimic the thin hypophase condition in the alveolus, we used an inverted coverslip setting. Cells cultured on a coverslip were placed upside-down on a drop of bath solution containing 300 nM PMA at the start of the experiment. Under these conditions, we found that individual LB fusion events in primary ATII cells were followed by FACE (Fig. 6, A, B, and D), indicating that ATP from LBs is sufficient to activate FACE in the absence of extracellular ATP. FACE was absent in primary ATII cells treated with VNUT shRNA for 3 d (Fig. 6, C and D). Quantitative analysis of the amplitude of the FACE signal (Miklavc et al., 2011) confirmed the full ablation of FACE in cells treated with VNUT shRNA (Fig. 6 D). We also analyzed the diffusion of FM1-43 across the fusion pore as a measure of fusion pore expansion/dilation (Miklavc et al., 2011). Diffusion of FM1-43 into vesicles fusing in control cells was significantly faster ( $P = 0.01$ ) compared with diffusion into fused LBs in cells treated with VNUT shRNA (Fig. 6 E). In summary, these data confirm that ATP from LBs activates vesicular  $\text{P2X}_4$  receptors and induces FACE (Fig. 7) in the absence of (exogenous) extracellular ATP.

## DISCUSSION

ATP is a major stimulus for LB exocytosis and surfactant secretion. Besides activation of FACE after LB fusion with the PM, extracellular ATP also triggers LB exocytosis via activation of  $\text{P2Y}_2$  and an increase in  $[\text{Ca}^{2+}]_i$  (Haller et al., 1999; Frick et al., 2001; Dietl et al., 2010). However, the reported concentration of ATP in the pulmonary hypophase is in the low nanomolar range under resting conditions (Patel et al., 2005; Bove et al., 2010) and well below the  $\text{EC}_{50}$  values for  $\text{P2Y}_2$  and  $\text{P2X}_4$  activation (Lazarowski et al., 1995; North, 2002; Abbracchio et al., 2006; Brunschweiler and Müller, 2006). Therefore, specific mechanisms are required to increase ATP concentrations within the alveoli of the lung. In particular, ATP is required to stimulate FACE and facilitate surfactant secretion after LB exocytosis. So far, however, ATP release in the alveoli has been observed mainly under conditions of increased respiration (e.g., as a consequence of exercise) or under pathological conditions.

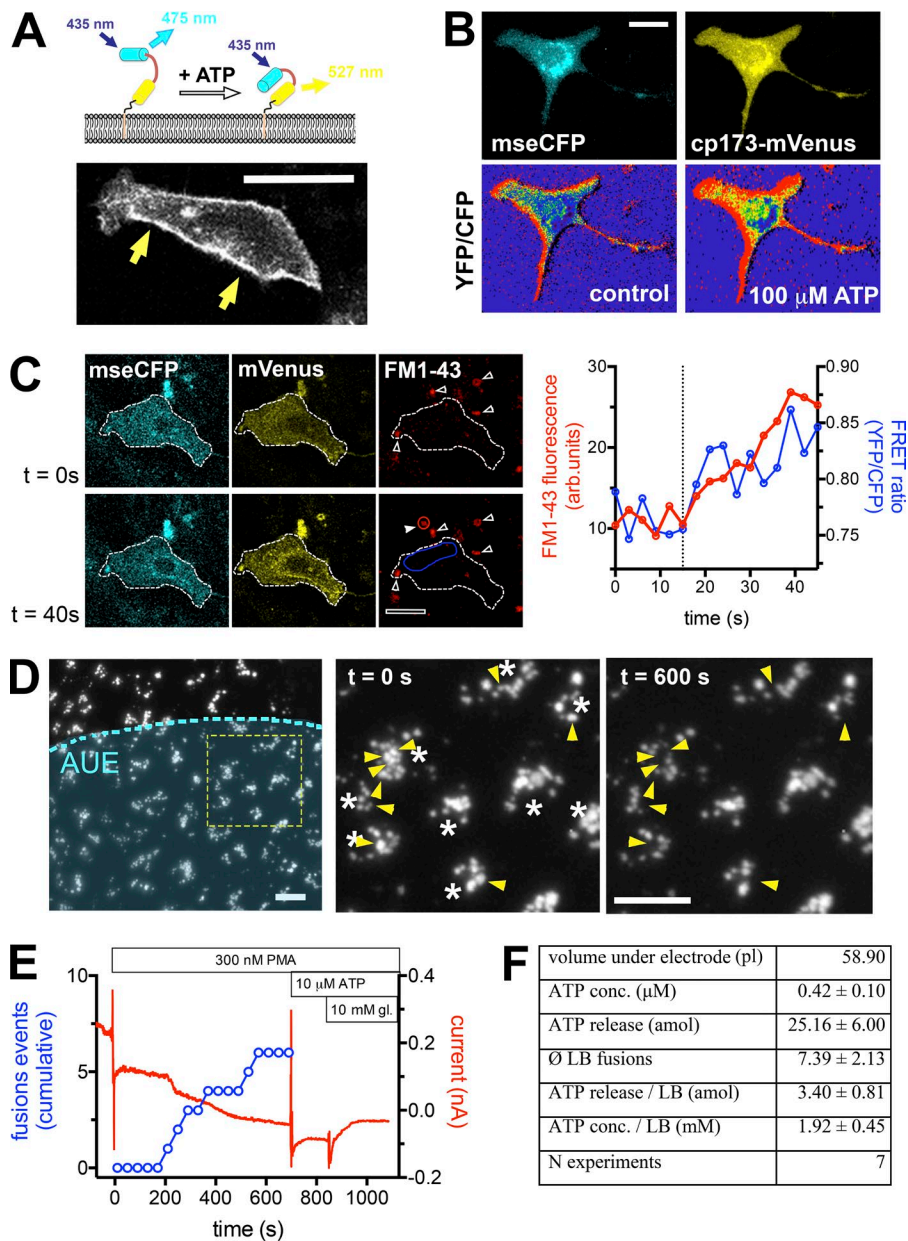


**Figure 5. ATP is released from individual LBs upon exocytosis. (A–C)** Detection of LB fusion-induced ATP release using genetically encoded ATP sensors. (A) Top: Schematic drawing of ATeam3.10-GL-GPI. Original ATeam3.10 is attached to a GPI-anchor (orange) via a 12xGlycin-linker (black) to facilitate selective expression in the outer leaflet of PM. Bottom: Image illustrating expression of ATeam3.10-GL-GPI on the cell surface (arrows) of ATII cells. Bar, 10 μm. (B) Images of the CFP (mseCFP) and YFP (cp173-mVenus) channel recorded from ATII cell expressing ATeam3.10-GL-GPI. Bottom: Representative YFP/CFP ratio images in the presence of 0 (control) and 100 μM extracellular ATP. Bar, 10 μm. (C) Left: ATeam3.10-GL-GPI was expressed in the outer leaflet of the PM in ATII cells (mseCFP, mVenus). FM1-43 selectively labels LBs after their fusion with the PM (arrowheads; empty arrowheads indicate FM1-43-positive LBs that fused to the PM before the start of the experiment; filled arrowhead indicates LB that fused during the experiment; Haller et al., 1998). Red circle (fused LB) denotes the region where the increase of FM1-43 fluorescence was analyzed. The area within the blue border represents the area where changes in the FRET ratio were analyzed. Bar, 10 μm. Right: Time course of FRET ratio (blue) and FM1-43 fluorescence (red) within the respective areas illustrated in the image on the left. Cells were stimulated at t = 0 s with 300 nM PMA. Dotted line indicates time of LB fusion (onset of FM1-43 fluorescence increase). (D–F) Quantitative analysis of ATP release from individual LBs. (D) Left: Image depicting ATII cells labeled with LTG. The blue shaded area indicates the area under the dual sensor electrode (AUE). LB fusion events were analyzed within the AUE. Middle and right: Magnified view of the area within

the yellow rectangle in the left image at t = 0 and 600 s after stimulation of ATII cells with 300 nM PMA. Arrowheads indicate LB that fused within the time course of the experiment (loss of LTG fluorescence in image, t = 600 s). Asterisks denote nuclei of individual primary ATII cells. Bars, 20 μm. (E) Time-current graph recorded with an ATP microbiosensor and cumulative LB fusion activity after stimulation of ATII cells with 300 nM PMA at t = 0 s. Fusion activity starts at  $\approx t = 180$  s and is accompanied by a decrease in current. Addition of ATP (10 μM, t = 700 s) results in a decrease in current, whereas addition of glucose (10 mM, t = 850 s) increases the current. (F) Table representing mean ATP release and LB fusion activity under the electrode from seven independent experiments (as illustrated in C). Based on the observed increase in ATP concentration under the electrode after LB fusions, we calculated a mean ATP concentration of 1.9 mM within individual LBs.

ATP is released from primary alveolar type I (ATI) cells or immortalized alveolar cells in response to increased alveolar distension (Patel et al., 2005; Mishra et al., 2011) or when coming in close proximity to the air-liquid interphase after a decrease in alveolar hypophase height (i.e., because of increased surface tension forces; Ramsingh et al., 2011), respectively. In line with this, a recent study found that mechanical ventilation resulted

in inflation-induced ATP release in the ex vivo rat lung, likely as a result of alveolar overdistension and stretch of alveolar cells (Furuya et al., 2016). This is also in line with the longstanding paradigm that cell stretch during deep inflation is the most potent stimulus for surfactant secretion (Mead and Collier, 1959; Wirtz and Dobbs, 2000; Dietl et al., 2004, 2010; Frick et al., 2004). Release of purine nucleotides from respiratory epithelia

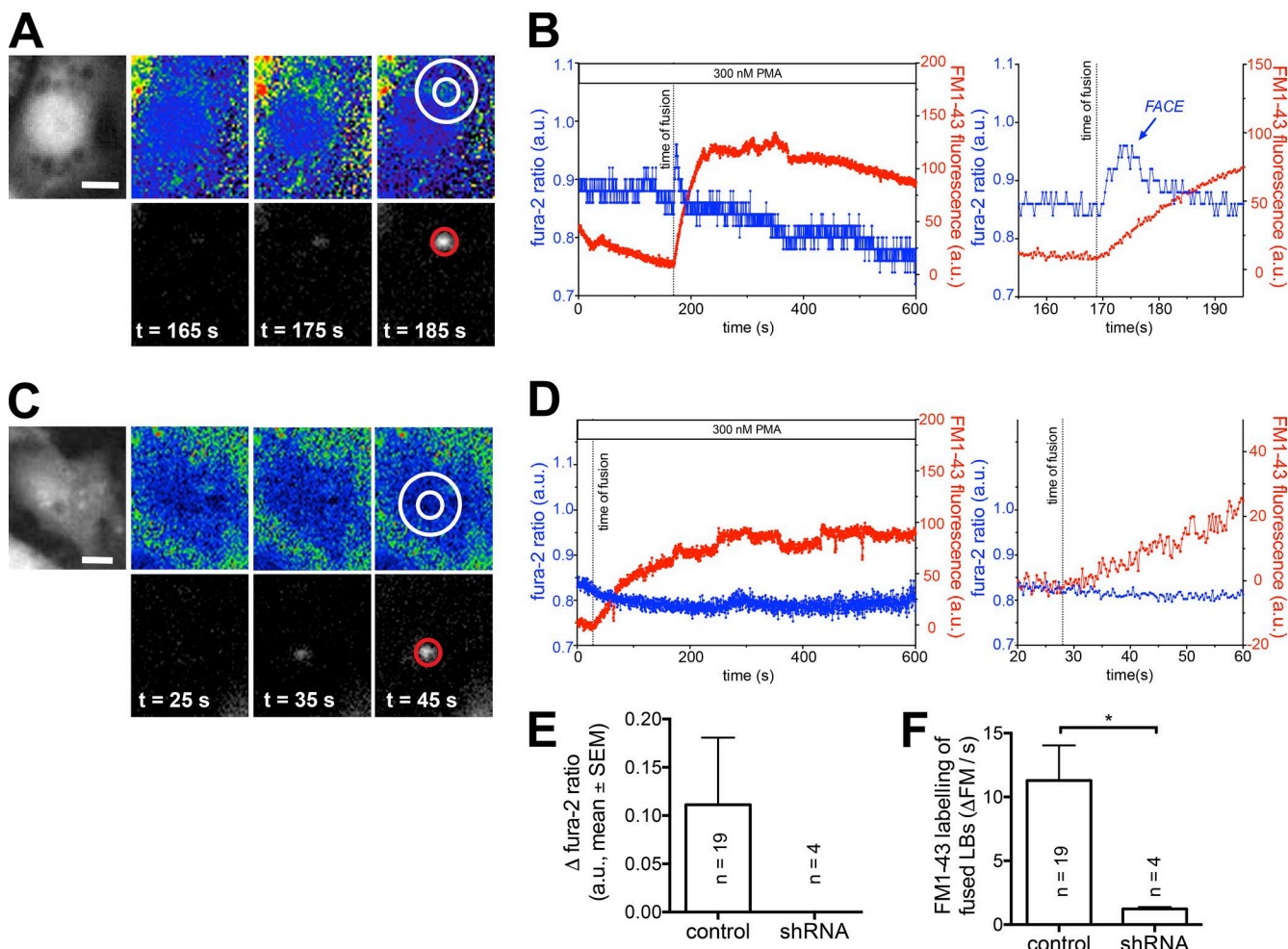


**Figure 6. Vesicular ATP activates FACE in an autocrine fashion upon LB exocytosis.** (A) Image sequence illustrating analysis of FACE in a cell loaded with Fura-2 and maintained in a bath containing FM1-43 (top left). Fura-2 ratios (top row) and FM1-43 fluorescence (bottom row) were acquired at 3 Hz. Red circle denotes the region where the increase of FM1-43 fluorescence was measured after fusion of LB with the PM. The area within the two white circles represents the ring-like region of interest surrounding the fused LB, where changes in  $[Ca^{2+}]_i$  (fura-2 ratio) were analyzed. *t*, time after start of experiment. Bar, 5  $\mu$ m. (B) Time course of fura-2 ratio (blue) and FM1-43 fluorescence (red) around and within the area of the LB fusion depicted in A. The cell was stimulated with 300 nM PMA. (C) Same as A, recorded in a cell treated with VNUT shRNA for 3 d. *t*, time after start of experiment. Bar, 5  $\mu$ m. (D) Time course of fura-2 ratio (blue) and FM1-43 fluorescence (red) around and within the area of the LB fusion depicted in C. The cell was stimulated with 300 nM PMA. Note the absence of FACE. (E) Quantitative analysis of the amplitude of the FACE signal from the experiments in B and D confirm full ablation of FACE in cells treated with VNUT shRNA. *n*, number of fusions analyzed for each condition. (F) Diffusion of FM1-43 into LBs after fusing with the PM.  $\Delta$  FM/s represents the slope of the increase in FM1-43 fluorescence of a fused vesicle in the first 10 s after fusion with the PM. This is a measure for initial diffusion of FM1-43 into a fused LB and correlates well with fusion pore diameter (Haller et al., 2001; Miklavc et al., 2011). FM1-43 diffusion was significantly faster (\*,  $P = 0.01$ ) in control cells compared with diffusion in cells treated with VNUT shRNA. *n*, number of fusions analyzed for each condition. Mean  $\pm$  SEM is shown.

is also significantly increased under pathophysiological conditions resulting from many chronic lung diseases (Adriaensen and Timmermans, 2004; Lommatzsch et al., 2010) or after trauma-induced damage of the alveolus (Riteau et al., 2010; Belete et al., 2011). Within this study, we now provide the first evidence for regulated ATP release from alveolar epithelial cells that could also be active under resting conditions. Surfactant is secreted constitutively under normal physiological conditions (i.e., to replace the surfactant cleared by macrophages, recycled by ATII cells or removed via

the mucociliary escalator; Perez-Gil and Weaver, 2010). Therefore, ATP is released from fused LBs to facilitate surfactant secretion in an autocrine fashion. Such local ATP release within individual alveoli may provide an ideal mechanism to gradually adapt local surfactant secretion to local demands and facilitate constitutive secretion of surfactant required to maintain the surfactant pool within the respiratory zone.

In addition, our results, together with the finding that ATP is released from ATI cells in response to increased inflation and alveolar distension (Patel et al.,

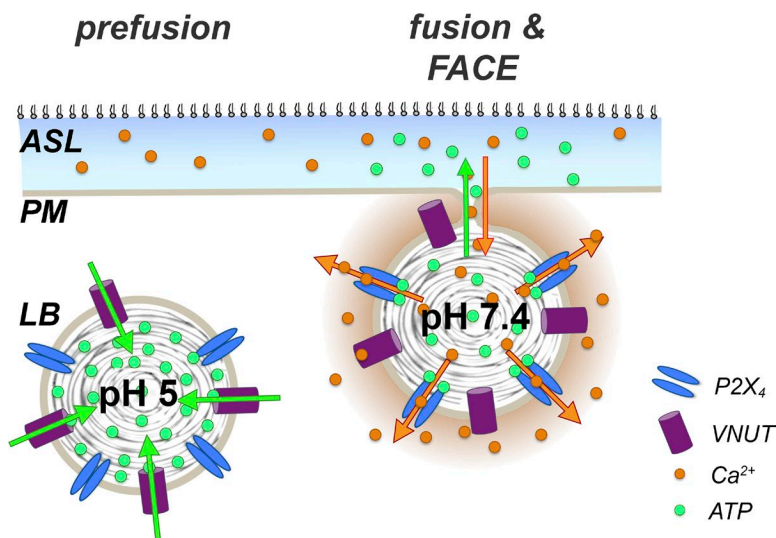


Figure 7. Schematic model of autocrine P2X<sub>4</sub> activation by vesicular ATP. P2X<sub>4</sub> is expressed on the limiting membrane of LBs, and ATP (green) is loaded into LBs by VNUT. The low pH within LBs protects P2X<sub>4</sub> from premature activation. Upon exocytosis and opening of the fusion pore, the pH within the lumen of the fused LB rises and P2X<sub>4</sub> receptors are activated by ATP, resulting in “fusion-activated Ca<sup>2+</sup>-entry” (FACE) at the site of LB fusion. FACE then facilitates fusion pore dilation, surfactant secretion, and fluid resorption from alveoli.

2005; Mishra et al., 2011) and that ATP is released as a “danger molecule” in response to alveolar damage (Riteau et al., 2010; Belete et al., 2011), indicate a delicate network to tightly regulate (“titrate and locate”) the extracellular ATP concentration within individual alveoli in response to specific intrinsic and extrinsic signals. A similar finding comes from the pancreatic duct (also a discrete physiological unit), where ATP is released by several mechanisms in response to various stimuli to maintain pancreatic duct homeostasis (Kowal et al., 2015). Moreover, such a network would be ideally suited to prevent excessive ATP release. This could be particularly important under disease conditions. P2X receptor expression is up-regulated in states of inflammation or tumor growth and/or after injury (Burnstock and Kennedy, 2011; Hafner et al., 2015). Up-regulated P2X expression might be linked to a chronic elevation of extracellular ATP (Geisler et al., 2013). Smoke-induced inflammation leads to increased levels of ATP in bronchoalveolar fluid and up-regulation of P2X<sub>7</sub> expression in the lung (Lommatzsch et al., 2010; Lucattelli et al., 2011). Therefore, P2X receptors may play an even greater role in pathological conditions with chronically increased extracellular ATP levels (Miklavc et al., 2013).

Our observation that ATP is stored in LBs is in line with findings that many secretory vesicles, including lysosome-related organelles and mucin granules in secretory airway cells, contain significant amounts of ATP (Bodin and Burnstock, 2001; Praetorius and Leipziger, 2009; Lazarowski et al., 2011; Estévez-Herrera et al., 2016). The calculated ATP concentration of 1.9 mM within the lumen of LBs is well in line with findings from acidic organelles in other cells (Huang et al., 2014). However, the concentration was calculated based on the amount of ATP released from individual LBs and assuming a homogeneous distribution of ATP within the volume of LBs. This likely leads to an underestimation of the actual ATP concentration within

the solute fraction inside individual LBs, as most of the LB volume (~95%) is occupied by lipids. Such accumulation of ATP within the solute fraction would also explain the bright fluorescence labeling of LBs compared with the cytoplasm after metabolic loading of AII cells with BODIPY FL ATP. Also, it is possible that not all ATP is released at once because of some compartmentalization within the LB (e.g., solute fraction vs. lipid contents vs. proteinaceous core). This could also explain why inhibition of VNUT by Evans Blue or bafilomycin A treatment results in almost complete block of ATP release despite the presence of some BODIPY FL ATP inside LBs. It is well established that LB contents (i.e., surfactant) are not readily released upon fusion pore opening and that release of the bulky cargo can be delayed for several minutes (Miklavc et al., 2012, 2015). Hence ATP “trapped” within an inner core might be released with considerable delay.

We reason that the main function of ATP in LBs is the efficient activation of P2X<sub>4</sub> receptors (and FACE) after LB exocytosis, but we cannot rule out additional functions of the intraorganelle colocalization of ATP and P2X<sub>4</sub> receptors in LBs. It has recently been demonstrated that endolysosomal P2X<sub>4</sub> forms channels activated by luminal ATP in a pH-dependent manner (Huang et al., 2014) and that P2X<sub>4</sub>-mediated endolysosomal Ca<sup>2+</sup> release promotes lysosome fusion (Cao et al., 2015). Although neutralization of the intra-LB pH resulted in a transient rise of the cytoplasmic Ca<sup>2+</sup> concentration around LBs, we did not observe fusions of intracellular LBs in our experiments. However, we cannot exclude that similar mechanisms are relevant during LB biogenesis or, alternatively, that alkalization as a result of cell damage promotes a massive Ca<sup>2+</sup> release from LBs to induce autophagy (La Rovere et al., 2016). It has also been suggested that vesicular ATP is essential to accumulate and concentrate neurotransmitters in secretory granules (Estévez-Herrera et al., 2016). This is

a rather unlikely for ATP in LBs, given that the main contents of LBs are lipids that are arranged in highly organized and tightly packed lamellar layers around a proteinaceous core (Vanhecke et al., 2010).

In summary, our results indicate that ATP is accumulated in LBs via VNUT. The low pH within the LB lumen prevents premature activation of P2X<sub>4</sub> receptors expressed in the LB membrane. The rise in intravesicular pH after opening of the exocytic fusion pore results in immediate activation of vesicular P2X<sub>4</sub> by vesicular ATP (Fig. 7). This colocalization of agonist (ATP) and receptor (P2X<sub>4</sub>) within single LBs ensures a highly specific, spatially and temporally controlled activation of P2X<sub>4</sub> receptors to promote FACE and facilitate secretion of pulmonary surfactant.

This is, to our knowledge, the first study demonstrating that receptor and ligand are colocalized in the same intracellular compartment, to ensure physiologically relevant receptor activation after coordinated secretion of receptor and ligand. It is very tempting to speculate that this mechanism is not unique to AII cells but constitutes a more general mechanism to regulate secretion, particularly in lysosome-related organelles. It has been shown that ATP is stored in insulin-containing granules in a VNUT-dependent manner. Knockdown of VNUT and/or decreased vesicular ATP release resulted in decreased P2X-dependent, glucose-sensitive insulin secretion in  $\beta$  cells (Geisler et al., 2013). It needs to be shown, however, whether P2X receptors are also localized on insulin secreting granules. Furthermore, our data provide a new model for ATP release from primary alveolar epithelial cells.

## ACKNOWLEDGMENTS

We thank T. Felder and A. Riecker for technical assistance, in particular for primary alveolar type II cell isolation, and S. Britsch and C. Wiegrefe for access to and support for the Leica SP5 confocal microscope.  $\alpha$ -VNUT pAB serum was a gift from Y. Moriyama. VNUT-GFP was a gift from T. Tsuboi. Plasmid P2X<sub>4</sub>-EGFP (WT) was a gift from R.D. Murrell-Lagnado, and plasmids encoding ATeam ATP sensors were a gift from H. Imamura.

This work was supported by a grant from the Ministry of Science, Research and the Arts of Baden-Württemberg (Az: 32-7533.-6-10/15/5) and Deutsche Forschungsgemeinschaft (DFG) grant DI1402/3-1 and grant SFB 1149/1, A05 to M. Frick. C. Kranz acknowledges funding from DFG (Graduierten Kolleg "Pulmosens").

The authors declare no competing financial interests.

Author contributions: M. Frick designed the study. All authors performed experiments and analyzed data. G. Fois, C. Kranz, and M. Frick wrote the manuscript.

Kenton J. Swartz served as editor.

Submitted: 3 August 2017

Revised: 12 October 2017

Accepted: 17 November 2017

## REFERENCES

Abbracchio, M.P., G. Burnstock, J.M. Boeynaems, E.A. Barnard, J.L. Boyer, C. Kennedy, G.E. Knight, M. Fumagalli, C. Gachet,

- K.A. Jacobson, and G.A. Weisman. 2006. International Union of Pharmacology LVIII: update on the P2Y G protein-coupled nucleotide receptors: From molecular mechanisms and pathophysiology to therapy. *Pharmacol. Rev.* 58:281–341. <https://doi.org/10.1124/pr.58.3.3>
- Adriaensen, D., and J.P. Timmermans. 2004. Purinergic signalling in the lung: Important in asthma and COPD? *Curr. Opin. Pharmacol.* 4:207–214. <https://doi.org/10.1016/j.coph.2004.01.010>
- Andronescu, C., S. Poller, and W. Schuhmann. 2014. Electrochemically induced deposition of poly(benzoxazine) precursors as immobilization matrix for enzymes. *Electrochem. Commun.* 41:12–15. <https://doi.org/10.1016/j.elecom.2014.01.015>
- Belete, H.A., R.D. Hubmayr, S. Wang, and R.D. Singh. 2011. The role of purinergic signaling on deformation induced injury and repair responses of alveolar epithelial cells. *PLoS One.* 6:e27469. <https://doi.org/10.1371/journal.pone.0027469>
- Bodin, P., and G. Burnstock. 2001. Purinergic signalling: ATP release. *Neurochem. Res.* 26:959–969. <https://doi.org/10.1023/A:1012388618693>
- Bove, P.F., B.R. Grubb, S.F. Okada, C.M. Ribeiro, T.D. Rogers, S.H. Randell, W.K. O'Neal, and R.C. Boucher. 2010. Human alveolar type II cells secrete and absorb liquid in response to local nucleotide signaling. *J. Biol. Chem.* 285:34939–34949. <https://doi.org/10.1074/jbc.M110.162933>
- Breckenridge, L.J., and W. Almers. 1987. Final steps in exocytosis observed in a cell with giant secretory granules. *Proc. Natl. Acad. Sci. USA.* 84:1945–1949. <https://doi.org/10.1073/pnas.84.7.1945>
- Brunschweiler, A., and C.E. Müller. 2006. P2 receptors activated by uracil nucleotides—An update. *Curr. Med. Chem.* 13:289–312. <https://doi.org/10.2174/092986706775476052>
- Burnstock, G., and C. Kennedy. 2011. P2X receptors in health and disease. *Adv. Pharmacol.* 61:333–372. <https://doi.org/10.1016/B978-0-12-385526-8.00011-4>
- Burnstock, G., A. Nistri, B.S. Khakh, and R. Giniatullin. 2014. ATP-gated P2X receptors in health and disease. *Front. Cell. Neurosci.* 8:204. <https://doi.org/10.3389/fncel.2014.00204>
- Cao, Q., K. Zhao, X.Z. Zhong, Y. Zou, H. Yu, P. Huang, T.L. Xu, and X.P. Dong. 2014. SLC17A9 protein functions as a lysosomal ATP transporter and regulates cell viability. *J. Biol. Chem.* 289:23189–23199. <https://doi.org/10.1074/jbc.M114.567107>
- Cao, Q., X.Z. Zhong, Y. Zou, R. Murrell-Lagnado, M.X. Zhu, and X.P. Dong. 2015. Calcium release through P2X4 activates calmodulin to promote endolysosomal membrane fusion. *J. Cell Biol.* 209:879–894. <https://doi.org/10.1083/jcb.201409071>
- Dietl, P., and T. Haller. 2005. Exocytosis of lung surfactant: From the secretory vesicle to the air-liquid interface. *Annu. Rev. Physiol.* 67:595–621. <https://doi.org/10.1146/annurev.physiol.67.040403.102553>
- Dietl, P., M. Frick, N. Mair, C. Bertocchi, and T. Haller. 2004. Pulmonary consequences of a deep breath revisited. *Biol. Neonate.* 85:299–304. <https://doi.org/10.1159/000078176>
- Dietl, P., B. Liss, E. Felder, P. Miklavc, and H. Wirtz. 2010. Lamellar body exocytosis by cell stretch or purinergic stimulation: possible physiological roles, messengers and mechanisms. *Cell. Physiol. Biochem.* 25:1–12. <https://doi.org/10.1159/000272046>
- Dietl, P., T. Haller, and M. Frick. 2012. Spatio-temporal aspects, pathways and actions of Ca(2+) in surfactant secreting pulmonary alveolar type II pneumocytes. *Cell Calcium.* 52:296–302. <https://doi.org/10.1016/j.ceca.2012.04.010>
- Dobbs, L.G., R. Gonzalez, and M.C. Williams. 1986. An improved method for isolating type II cells in high yield and purity. *Am. Rev. Respir. Dis.* 134:141–145.

- Erb, L., Z. Liao, C.I. Seye, and G.A. Weisman. 2006. P2 receptors: Intracellular signaling. *Pflugers Arch.* 452:552–562. <https://doi.org/10.1007/s00424-006-0069-2>
- Estévez-Herrera, J., N. Domínguez, M.R. Pardo, A. González-Santana, E.W. Westhead, R. Borges, and J.D. Machado. 2016. ATP: The crucial component of secretory vesicles. *Proc. Natl. Acad. Sci. USA.* 113:E4098–E4106. <https://doi.org/10.1073/pnas.1600690113>
- Fois, G., N. Hobi, E. Felder, A. Ziegler, P. Miklavc, P. Walther, P. Radermacher, T. Haller, and P. Dietl. 2015. A new role for an old drug: Ambroxol triggers lysosomal exocytosis via pH-dependent Ca<sup>2+</sup> release from acidic Ca<sup>2+</sup> stores. *Cell Calcium.* 58:628–637. <https://doi.org/10.1016/j.ceca.2015.10.002>
- Frick, M., S. Eschertzhuber, T. Haller, N. Mair, and P. Dietl. 2001. Secretion in alveolar type II cells at the interface of constitutive and regulated exocytosis. *Am. J. Respir. Cell Mol. Biol.* 25:306–315. <https://doi.org/10.1165/ajrcmb.25.3.4493>
- Frick, M., C. Bertocchi, P. Jennings, T. Haller, N. Mair, W. Singer, W. Pfaller, M. Ritsch-Marte, and P. Dietl. 2004. Ca<sup>2+</sup> entry is essential for cell strain-induced lamellar body fusion in isolated rat type II pneumocytes. *Am. J. Physiol. Lung Cell. Mol. Physiol.* 286:L210–L220. <https://doi.org/10.1152/ajplung.00332.2003>
- Furuya, K., J.J. Tan, F. Boudreault, M. Sokabe, Y. Berthiaume, and R. Grygorczyk. 2016. Real-time imaging of inflation-induced ATP release in the ex vivo rat lung. *Am. J. Physiol. Lung Cell. Mol. Physiol.* 311:L956–L969. <https://doi.org/10.1152/ajplung.00425.2015>
- Geisler, J.C., K.L. Corbin, Q. Li, A.P. Feranchak, C.S. Nunemaker, and C. Li. 2013. Vesicular nucleotide transporter-mediated ATP release regulates insulin secretion. *Endocrinology.* 154:675–684. <https://doi.org/10.1210/en.2012-1818>
- Gou, D., A. Mishra, T. Weng, L. Su, N.R. Chintagari, Z. Wang, H. Zhang, L. Gao, P. Wang, H.M. Stricker, and L. Liu. 2008. Annexin A2 interactions with Rab14 in alveolar type II cells. *J. Biol. Chem.* 283:13156–13164. <https://doi.org/10.1074/jbc.M801532200>
- Haanes, K.A., and I. Novak. 2010. ATP storage and uptake by isolated pancreatic zymogen granules. *Biochem. J.* 429:303–311. <https://doi.org/10.1042/BJ20091337>
- Hafner, S., K. Wagner, M. Wepler, J. Matallo, M. Gröger, O. McCook, A. Scheuerle, M. Huber-Lang, M. Frick, S. Weber, et al. 2015. Physiological and immune-biological characterization of a long-term murine model of blunt chest trauma. *Shock.* 43:140–147. <https://doi.org/10.1097/SHK.0000000000000277>
- Haller, T., J. Ortmayr, F. Friedrich, H. Völkl, and P. Dietl. 1998. Dynamics of surfactant release in alveolar type II cells. *Proc. Natl. Acad. Sci. USA.* 95:1579–1584. <https://doi.org/10.1073/pnas.95.4.1579>
- Haller, T., K. Auktor, M. Frick, N. Mair, and P. Dietl. 1999. Threshold calcium levels for lamellar body exocytosis in type II pneumocytes. *Am. J. Physiol.* 277:L893–L900.
- Haller, T., P. Dietl, K. Pfaller, M. Frick, N. Mair, M. Paulmichl, M.W. Hess, J. Furst, and K. Maly. 2001. Fusion pore expansion is a slow, discontinuous, and Ca<sup>2+</sup>-dependent process regulating secretion from alveolar type II cells. *J. Cell Biol.* 155:279–289. <https://doi.org/10.1083/jcb.200102106>
- Huang, P., Y. Zou, X.Z. Zhong, Q. Cao, K. Zhao, M.X. Zhu, R. Murrell-Lagnado, and X.P. Dong. 2014. P2X4 forms functional ATP-activated cation channels on lysosomal membranes regulated by luminal pH. *J. Biol. Chem.* 289:17658–17667. <https://doi.org/10.1074/jbc.M114.552158>
- Imamura, H., K.P. Nhat, H. Togawa, K. Saito, R. Iino, Y. Kato-Yamada, T. Nagai, and H. Noji. 2009. Visualization of ATP levels inside single living cells with fluorescence resonance energy transfer-based genetically encoded indicators. *Proc. Natl. Acad. Sci. USA.* 106:15651–15656. <https://doi.org/10.1073/pnas.0904764106>
- Imura, Y., Y. Morizawa, R. Komatsu, K. Shibata, Y. Shinozaki, H. Kasai, K. Moriishi, Y. Moriyama, and S. Koizumi. 2013. Microglia release ATP by exocytosis. *Glia.* 61:1320–1330. <https://doi.org/10.1002/glia.22517>
- Keller, P., D. Toomre, E. Díaz, J. White, and K. Simons. 2001. Multicolour imaging of post-Golgi sorting and trafficking in live cells. *Nat. Cell Biol.* 3:140–149. <https://doi.org/10.1038/35055042>
- Kowal, J.M., G.G. Yegutkin, and I. Novak. 2015. ATP release, generation and hydrolysis in exocrine pancreatic duct cells. *Purinergic Signal.* 11:533–550. <https://doi.org/10.1007/s11302-015-9472-5>
- Kreda, S.M., L. Seminario-Vidal, C.A. van Heusden, W. O’Neal, L. Jones, R.C. Boucher, and E.R. Lazarowski. 2010. Receptor-promoted exocytosis of airway epithelial mucin granules containing a spectrum of adenine nucleotides. *J. Physiol.* 588:2255–2267. <https://doi.org/10.1113/jphysiol.2009.186643>
- La Rovere, R.M., G. Roest, G. Bultynck, and J.B. Parys. 2016. Intracellular Ca(2+) signaling and Ca(2+) microdomains in the control of cell survival, apoptosis and autophagy. *Cell Calcium.* 60:74–87. <https://doi.org/10.1016/j.ceca.2016.04.005>
- Lazarowski, E.R. 2012. Vesicular and conductive mechanisms of nucleotide release. *Purinergic Signal.* 8:359–373. <https://doi.org/10.1007/s11302-012-9304-9>
- Lazarowski, E.R., W.C. Watt, M.J. Stutts, R.C. Boucher, and T.K. Harden. 1995. Pharmacological selectivity of the cloned human P2U-purinoceptor: Potent activation by diadenosine tetraphosphate. *Br. J. Pharmacol.* 116:1619–1627. <https://doi.org/10.1111/j.1476-5381.1995.tb16382.x>
- Lazarowski, E.R., J.I. Sesma, L. Seminario-Vidal, and S.M. Kreda. 2011. Molecular mechanisms of purine and pyrimidine nucleotide release. *Adv. Pharmacol.* 61:221–261. <https://doi.org/10.1016/B978-0-12-385526-8.00008-4>
- Lommatzsch, M., S. Cicko, T. Müller, M. Lucattelli, K. Bratke, P. Stoll, M. Grimm, T. Dürk, G. Zissel, D. Ferrari, et al. 2010. Extracellular adenosine triphosphate and chronic obstructive pulmonary disease. *Am. J. Respir. Crit. Care Med.* 181:928–934. <https://doi.org/10.1164/rccm.200910-1506OC>
- Lucattelli, M., S. Cicko, T. Müller, M. Lommatzsch, G. De Cunto, S. Cardini, W. Sundas, M. Grimm, R. Zeiser, T. Dürk, et al. 2011. P2X7 receptor signaling in the pathogenesis of smoke-induced lung inflammation and emphysema. *Am. J. Respir. Cell Mol. Biol.* 44:423–429. <https://doi.org/10.1165/rcmb.2010-0038OC>
- Masson, J.F., E. Gauda, B. Mizaiikoff, and C. Kranz. 2008. The interference of HEPES buffer during amperometric detection of ATP in clinical applications. *Anal. Bioanal. Chem.* 390:2067–2071. <https://doi.org/10.1007/s00216-008-2015-y>
- Mead, J., and C.R. Collier. 1959. Relation of volume history of lungs to respiratory mechanics in anaesthetized dogs. *J. Appl. Physiol.* 14:669–678.
- Miklavc, P., M. Frick, O.H. Wittekindt, T. Haller, and P. Dietl. 2010. Fusion-activated Ca(2+) entry: An “active zone” of elevated Ca(2+) during the postfusion stage of lamellar body exocytosis in rat type II pneumocytes. *PLoS One.* 5:e10982. <https://doi.org/10.1371/journal.pone.0010982>
- Miklavc, P., N. Mair, O.H. Wittekindt, T. Haller, P. Dietl, E. Felder, M. Timmler, and M. Frick. 2011. Fusion-activated Ca<sup>2+</sup> entry via vesicular P2X4 receptors promotes fusion pore opening and exocytotic content release in pneumocytes. *Proc. Natl. Acad. Sci. USA.* 108:14503–14508. <https://doi.org/10.1073/pnas.1101039108>
- Miklavc, P., E. Hecht, N. Hobi, O.H. Wittekindt, P. Dietl, C. Kranz, and M. Frick. 2012. Actin coating and compression of fused secretory vesicles are essential for surfactant secretion—A role

- for Rho, formins and myosin II. *J. Cell Sci.* 125:2765–2774. <https://doi.org/10.1242/jcs.105262>
- Miklavc, P., K.E. Thompson, and M. Frick. 2013. A new role for P2X4 receptors as modulators of lung surfactant secretion. *Front. Cell. Neurosci.* 7:171. <https://doi.org/10.3389/fncel.2013.00171>
- Miklavc, P., K. Ehinger, A. Sultan, T. Felder, P. Paul, K.E. Gottschalk, and M. Frick. 2015. Actin depolymerisation and crosslinking join forces with myosin II to contract actin coats on fused secretory vesicles. *J. Cell Sci.* 128:1193–1203. <https://doi.org/10.1242/jcs.165571>
- Mishra, A., N.R. Chintagari, Y. Guo, T. Weng, L. Su, and L. Liu. 2011. Purinergic P2X7 receptor regulates lung surfactant secretion in a paracrine manner. *J. Cell Sci.* 124:657–668. <https://doi.org/10.1242/jcs.066977>
- Moriyama, Y., M. Hiasa, S. Sakamoto, H. Omote, and M. Nomura. 2017. Vesicular nucleotide transporter (VNUT): Appearance of an actress on the stage of purinergic signaling. *Purinergic Signal.* 13:387–404. <https://doi.org/10.1007/s11302-017-9568-1>
- Neuland, K., N. Sharma, and M. Frick. 2014. Synaptotagmin-7 links fusion-activated Ca<sup>2+</sup> entry and fusion pore dilation. *J. Cell Sci.* 127:5218–5227. <https://doi.org/10.1242/jcs.153742>
- North, R.A. 2002. Molecular physiology of P2X receptors. *Physiol. Rev.* 82:1013–1067. <https://doi.org/10.1152/physrev.00015.2002>
- Novak, I. 2011. Purinergic signalling in epithelial ion transport: Regulation of secretion and absorption. *Acta Physiol. (Oxf.)*. 202:501–522. <https://doi.org/10.1111/j.1748-1716.2010.02225.x>
- Obermüller, S., A. Lindqvist, J. Karanauskaite, J. Galvanovskis, P. Rorsman, and S. Barg. 2005. Selective nucleotide-release from dense-core granules in insulin-secreting cells. *J. Cell Sci.* 118:4271–4282. <https://doi.org/10.1242/jcs.02549>
- Okada, S.F., L. Zhang, S.M. Kreda, L.H. Abdullah, C.W. Davis, R.J. Pickles, E.R. Lazarowski, and R.C. Boucher. 2011. Coupled nucleotide and mucin hypersecretion from goblet-cell metaplastic human airway epithelium. *Am. J. Respir. Cell Mol. Biol.* 45:253–260. <https://doi.org/10.1165/rcmb.2010-0253OC>
- Oya, M., T. Kitaguchi, Y. Yanagihara, R. Numano, M. Kakeyama, K. Ikematsu, and T. Tsuboi. 2013. Vesicular nucleotide transporter is involved in ATP storage of secretory lysosomes in astrocytes. *Biochem. Biophys. Res. Commun.* 438:145–151. <https://doi.org/10.1016/j.bbrc.2013.07.043>
- Patel, A.S., D. Reigada, C.H. Mitchell, S.R. Bates, S.S. Margulies, and M. Koval. 2005. Paracrine stimulation of surfactant secretion by extracellular ATP in response to mechanical deformation. *Am. J. Physiol. Lung Cell. Mol. Physiol.* 289:L489–L496. <https://doi.org/10.1152/ajplung.00074.2005>
- Perez-Gil, J., and T.E. Weaver. 2010. Pulmonary surfactant pathophysiology: Current models and open questions. *Physiology (Bethesda)*. 25:132–141. <https://doi.org/10.1152/physiol.00006.2010>
- Pfaffl, M.W. 2001. A new mathematical model for relative quantification in real-time RT-PCR. *Nucleic Acids Res.* 29:e45. <https://doi.org/10.1093/nar/29.9.e45>
- Porat-Shliom, N., O. Milberg, A. Masedunskas, and R. Weigert. 2013. Multiple roles for the actin cytoskeleton during regulated exocytosis. *Cell. Mol. Life Sci.* 70:2099–2121. <https://doi.org/10.1007/s00018-012-1156-5>
- Praetorius, H.A., and J. Leipziger. 2009. ATP release from non-excitable cells. *Purinergic Signal.* 5:433–446. <https://doi.org/10.1007/s11302-009-9146-2>
- Ramsingh, R., A. Grygorczyk, A. Solecki, L.S. Cherkaoui, Y. Berthiaume, and R. Grygorczyk. 2011. Cell deformation at the air-liquid interface induces Ca<sup>2+</sup>-dependent ATP release from lung epithelial cells. *Am. J. Physiol. Lung Cell. Mol. Physiol.* 300:L587–L595. <https://doi.org/10.1152/ajplung.00345.2010>
- Ransford, G.A., N. Fregien, F. Qiu, G. Dahl, G.E. Conner, and M. Salathe. 2009. Pannexin 1 contributes to ATP release in airway epithelia. *Am. J. Respir. Cell Mol. Biol.* 41:525–534. <https://doi.org/10.1165/rcmb.2008-0367OC>
- Riteau, N., P. Gasse, L. Fauconnier, A. Gombault, M. Couegnat, L. Fick, J. Kanellopoulos, V.F. Quesniaux, S. Marchand-Adam, B. Crestani, et al. 2010. Extracellular ATP is a danger signal activating P2X7 receptor in lung inflammation and fibrosis. *Am. J. Respir. Crit. Care Med.* 182:774–783. <https://doi.org/10.1164/rccm.201003-0359OC>
- Sawada, K., N. Echigo, N. Juge, T. Miyaji, M. Otsuka, H. Omote, A. Yamamoto, and Y. Moriyama. 2008. Identification of a vesicular nucleotide transporter. *Proc. Natl. Acad. Sci. USA.* 105:5683–5686. <https://doi.org/10.1073/pnas.0800141105>
- Seminario-Vidal, L., S.F. Okada, J.I. Sesma, S.M. Kreda, C.A. van Heusden, Y. Zhu, L.C. Jones, W.K. O’Neal, S. Penuela, D.W. Laird, et al. 2011. Rho signaling regulates pannexin 1-mediated ATP release from airway epithelia. *J. Biol. Chem.* 286:26277–26286. <https://doi.org/10.1074/jbc.M111.260562>
- Sesma, J.I., S.M. Kreda, S.F. Okada, C. van Heusden, L. Moussa, L.C. Jones, W.K. O’Neal, N. Togawa, M. Hiasa, Y. Moriyama, and E.R. Lazarowski. 2013. Vesicular nucleotide transporter regulates the nucleotide content in airway epithelial mucin granules. *Am. J. Physiol. Cell Physiol.* 304:C976–C984. <https://doi.org/10.1152/ajpcell.00371.2012>
- Singer, W., M. Frick, T. Haller, S. Bernet, M. Ritsch-Marte, and P. Dietl. 2003. Mechanical forces impeding exocytotic surfactant release revealed by optical tweezers. *Biophys. J.* 84:1344–1351. [https://doi.org/10.1016/S0006-3495\(03\)74950-9](https://doi.org/10.1016/S0006-3495(03)74950-9)
- Sorensen, C.E., and I. Novak. 2001. Visualization of ATP release in pancreatic acini in response to cholinergic stimulus. Use of fluorescent probes and confocal microscopy. *J. Biol. Chem.* 276:32925–32932. <https://doi.org/10.1074/jbc.M103313200>
- Surprenant, A., and R.A. North. 2009. Signaling at purinergic P2X receptors. *Annu. Rev. Physiol.* 71:333–359. <https://doi.org/10.1146/annurev.physiol.70.113006.100630>
- Tatur, S., S. Kreda, E. Lazarowski, and R. Grygorczyk. 2008. Calcium-dependent release of adenosine and uridine nucleotides from A549 cells. *Purinergic Signal.* 4:139–146. <https://doi.org/10.1007/s11302-007-9059-x>
- Thompson, K.E., J.P. Korbmacher, E. Hecht, N. Hobi, O.H. Wittekindt, P. Dietl, C. Kranz, and M. Frick. 2013. Fusion-activated cation entry (FACE) via P2X<sub>4</sub> couples surfactant secretion and alveolar fluid transport. *FASEB J.* 27:1772–1783. <https://doi.org/10.1096/fj.12-220533>
- Vanhecke, D., G. Herrmann, W. Graber, T. Hillmann-Marti, C. Mühlfeld, D. Studer, and M. Ochs. 2010. Lamellar body ultrastructure revisited: High-pressure freezing and cryo-electron microscopy of vitreous sections. *Histochem. Cell Biol.* 134:319–326. <https://doi.org/10.1007/s00418-010-0736-4>
- Vardjan, N., M. Stenovc, J. Jorgacevski, M. Kreft, S. Grilc, and R. Zorec. 2009. The fusion pore and vesicle cargo discharge modulation. *Ann. N. Y. Acad. Sci.* 1152:135–144. <https://doi.org/10.1111/j.1749-6632.2008.04007.x>
- Wirtz, H.R., and L.G. Dobbs. 2000. The effects of mechanical forces on lung functions. *Respir. Physiol.* 119:1–17. [https://doi.org/10.1016/S0034-5687\(99\)00092-4](https://doi.org/10.1016/S0034-5687(99)00092-4)
- Xu, J., H. Chai, K. Ehinger, T.M. Egan, R. Srinivasan, M. Frick, and B.S. Khakh. 2014. Imaging P2X<sub>4</sub> receptor subcellular distribution,

trafficking, and regulation using P2X4-pHluorin. *J. Gen. Physiol.* 144:81–104. <https://doi.org/10.1085/jgp.201411169>

Ziller, C., J. Lin, P. Knittel, L. Friedrich, C. Andronescu, S. Poller, W. Schuhmann, and C. Kranz. 2017. Poly(benzoxazine) as

an immobilization matrix for miniaturized ATP and glucose biosensors. *ChemElectroChem.* 4:864–871. <https://doi.org/10.1002/celc.201600765>